Separation Science and Technology
Publication details, including instructions for authors and subscription information:
http://www.informaworld.com/smpp/title~content=t713708471

Groundwater Cleanup by In-Situ Sparging. VIII. Effect of Air Channeling on Dissolved Volatile Organic Compounds Removal Efficiency

David J. Wilson[a]; Cesar Gómez-Lahoz[a]; José M. Rodríguez-Maroto[a]
[a] DEPARTAMENTO DE INGENIERÍA QUÍMICA, FACULTAD DE CIENCIAS, CAMPUS UNIVERSITARIO DE TEÁTINOS, UNIVERSIDAD DE MÁLAGA, MÁLAGA, SPAIN

To cite this Article Wilson, David J. , Gómez-Lahoz, Cesar and Rodríguez-Maroto, José M.(1994) 'Groundwater Cleanup by In-Situ Sparging. VIII. Effect of Air Channeling on Dissolved Volatile Organic Compounds Removal Efficiency', Separation Science and Technology, 29: 18, 2387 — 2418
To link to this Article: DOI: 10.1080/01496399408002200
URL: http://dx.doi.org/10.1080/01496399408002200

SEPARATION SCIENCE AND TECHNOLOGY, **29**(18), pp. 2387–2418, 1994

Groundwater Cleanup by In-Situ Sparging. VIII. Effect of Air Channeling on Dissolved Volatile Organic Compounds Removal Efficiency

DAVID J. WILSON,* CESAR GÓMEZ-LAHOZ, and
JOSÉ M. RODRÍGUEZ-MAROTO
DEPARTAMENTO DE INGENIERÍA QUÍMICA
FACULTAD DE CIENCIAS
CAMPUS UNIVERSITARIO DE TEÁTINOS
UNIVERSIDAD DE MÁLAGA
29071 MÁLAGA, SPAIN

ABSTRACT

A mathematical model for removal of dissolved volatile organic compounds (VOCs) from contaminated aquifers by in-situ air sparging is described. The model assumes that the sparging air moves through persistent channels in the aquifer, and that VOC transport to the sparging air is by diffusion/dispersion and air-induced circulation of the water in the vicinity of the sparging well. The dependence of model results on the parameters of the model is explored. The use of pulsed air flow in sparging as a means to increase VOC transport by dispersion is suggested. An extension and modification of the Sellers–Schreiber preliminary screening model for in-situ air sparging is also described. The revised model includes an improved method for calculating bubble residence times in the aquifer, and also permits the modeling of nonaqueous phase liquid (NAPL) removal.

INTRODUCTION

In-situ air sparging (ISAS) is turning out to be quite effective in the remediation of hazardous waste sites at which groundwater is contaminated with volatile organic compounds (VOCs). Brown has given a rather

* Permanent address: Department of Chemistry, Box 1822, Sta. B, Vanderbilt University, Nashville, Tennessee 37235, USA.

complete introduction to sparging (1), Clarke et al. (2) have reviewed the technique, and an EPA report (3) includes articles on this method. Sellers and Schreiber (4) have listed a number of sites at which air sparging was used and at which groundwater cleanup goals were achieved in a year or less.

In two recent papers (5, 6) we developed mathematical models for describing ISAS by means of buried horizontal slotted pipes and by single vertical wells screened for a short distance at the bottom of the well. These analyses include the modeling of solution/diffusion process kinetics, and they permit one to model, for example, groundwater VOC concentration rebound resulting from diffusion of VOC after system shutdown.

In the sparging of small-scale water-saturated sand beds we have always noticed a certain persistence in time of the air bubble locations in the supernatant water at the top of the sand bed which is being sparged. Over a wide range of air flow rates we observed bubbles appearing over the surface of the sand bed at relatively random locations which persisted for extended periods of time. Evidently the bulk of the injected air was being conducted to the surface of the simulated aquifer along a limited number of preferred paths even in our highly homogeneous porous medium (plasterer's sand which had been washed free of dirt and clay). This may have unfortunate implications in terms of reduced VOC mass transfer efficiency since it implies that VOCs must move in the aqueous phase, probably mainly by diffusion and dispersion, to these air-carrying tubes in order to be removed.

In the present paper we develop a mathematical model for sparging in which the air is carried along persistent preferred channels and the dissolved VOC is moved by diffusion/dispersion to these channels for removal. The model follows rather closely along the lines of our previous work (5, 6), but it deals only with dissolved VOC and uses a quite different picture of diffusion/dispersion than was used earlier.

Here we first give a somewhat abbreviated derivation of the differential equations constituting the model in order to avoid repetition of analysis discussed previously (5, 6). (The new picture of diffusion/dispersion is discussed in full.) We then examine some results obtained with this model and indicate a possible technique for improving mass transfer by dispersion in sparging.

The paper closes with a discussion of a quite simple sparging model suitable for use in preliminary screening. This is a modification and extension of an approach developed earlier by Sellers and Schreiber (4) for preliminary screening.

THE MODEL FOR SPARGING WITH DISPERSION TRANSPORT

The overall geometry is that of a single sparging well, screened at the bottom and operating in a homogeneous, isotropic aquifer. We use cylindrical coordinates R and z; see Fig. 1.

We assume that the sparging air passes through the aquifer in persistent tubes or channels, and that dissolved VOC moves from the neighboring aqueous phase to the border of the tube of air-filled medium by diffusion/dispersion. Note that the rate of such mass transport by dispersion can perhaps be substantially enhanced by pulsed air flow. Let the number n_{ij} of such tubes passing through one of the ring-shaped volume elements ΔV_{ij} be proportional to $\Delta V_{ij}/\Delta z$ (the top or bottom surface area of the volume element) and to the molar air flux in the volume element,

$$q_{ij} = [q_r^2 + q_z^2]^{1/2}$$

The proportionality constant, K, is a measure of the ease with which channels form in the porous medium (and therefore of their number).

Let us focus on one volume element ΔV_{ij}, of height Δz and horizontal cross-sectional area $A_{ij} = \pi(R_{i+1}^2 - R_i^2)$, where $R_i = (i - 1)\Delta R$. There

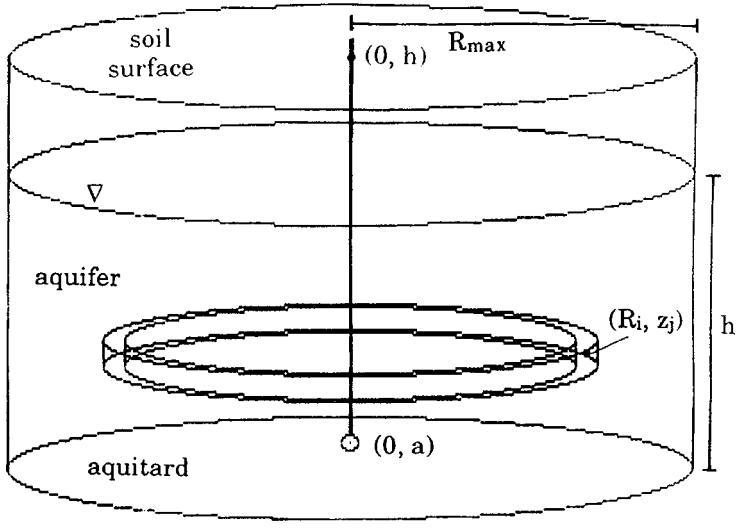

FIG. 1 Geometry and notation for a simple vertical sparging well screened at the bottom.

are n_{ij} tubes passing through this volume element, with

$$n_{ij} = KA_{ij}q_{ij} \tag{1}$$

We associate with each tube a cylindrical portion of the volume element of volume $\Delta V_{ij}/n_{ij}$. The radius of this subunit of ΔV_{ij} is given by

$$n_{ij}\pi b_{ij}^2 = A_{ij} \tag{2}$$

and substitution of Eq. (1) into Eq. (2) and rearrangement gives

$$b_{ij} = [\pi K q_{ij}]^{-1/2} \tag{3}$$

See Fig. 2.

We analyze diffusion transport from the small water-filled annular domain surrounding one of the air channels on the axis of this domain to the air-filled channel, as illustrated in the blow-up in Fig. 2. The subscripts i and j will be dropped for the moment. The water-filled domain is partitioned into a set of n_u concentric annular volume elements (shells) as indicated in Fig. 3. Here

$$\Delta u = \frac{b - a}{n_u} \left(\text{later, } \Delta u_{ij} = \frac{b_{ij} - a}{n_u} \right) \tag{4}$$

$$r_k = a + (k - 1)\Delta u \tag{5}$$

$$\Delta v_k = \pi \Delta z (r_{k+1}^2 - r_k^2) = \pi \Delta z [2a\Delta u + (2k - 1)(\Delta u)^2] \tag{6}$$

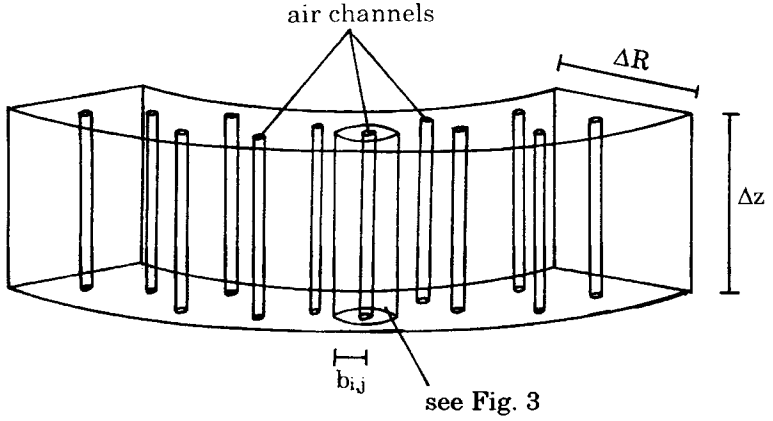

FIG. 2 Representative air channels and an associated domain in ΔV_{ij}.

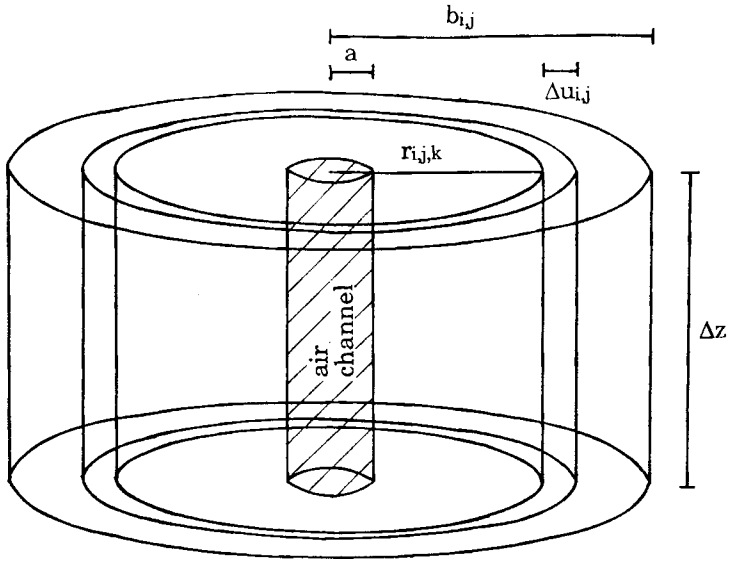

FIG. 3 Partitioning of the domain surrounding a single channel.

and ν = porosity of the medium

C_k^w = dissolved VOC concentration in the kth annular volume element

D = diffusivity/dispersivity of VOC in the water-saturated porous medium

Then

$$\nu \Delta v_k \frac{dC_k^w}{dt} = \frac{2\pi \Delta z D}{\Delta u} [r_k(C_{k-1}^w - C_k^w) + r_{k+1}(C_{k+1}^w - C_k^w)], \quad k = 2, 3, \ldots, n_u - 1 \tag{7}$$

and

$$\frac{dC_k^w}{dt} = \frac{2\pi \Delta z D}{\nu \Delta v_k \Delta u} [r_k(C_{k-1}^w - C_k^w) + r_{k+1}(C_{k+1}^w - C_k^w)] \tag{8}$$

For the outermost shell

$$\frac{dC_{nu}^w}{dt} = \frac{2\pi \Delta z D}{\nu \Delta v_k \Delta u} r_{nu}(C_{nu-1}^w - C_{nu}^w) \tag{9}$$

For the innermost shell

$$\frac{dC_1^w}{dt} = \frac{2\pi\Delta z D}{\nu\Delta v_1 \Delta u}\left[2a(C^g/K_H - C_1^w) + r_2(C_2^w - C_1^w)\right] \tag{10}$$

where C^g = vapor phase concentration of VOC in the air-filled tube
K_H = Henry's constant of VOC (dimensionless)

This completes the analysis of diffusion/dispersion transport in the aqueous phase.

We next turn to the examination of advective transport by the circulating water. Here we are dealing with large-scale circulation rather than small-scale eddies and turbulence which are handled by the dispersion treatment just completed. We re-introduce the subscripts i, j for the large ring-shaped volume elements ΔV_{ij}. In this subscript-laden notation, our previous equations become

$$\left[\frac{\partial C_{ijk}^w}{\partial t}\right]_{\text{disp}} = \frac{2D/\Delta u_{ij}}{\nu(r_{ij,k+1}^2 - r_{ijk}^2)} \times \left[r_{ijk}(C_{ij,k-1}^w - C_{ijk}^w) + r_{ij,k+1}(C_{ij,k+1}^w - C_{ijk}^w)\right] \tag{11}$$

$$\left[\frac{\partial C_{ij,nu}^w}{\partial t}\right]_{\text{disp}} = \frac{2D/\Delta u_{ij}}{\nu(r_{ij,nu+1}^2 - r_{ij,nu}^2)}\left[r_{ij,nu}(C_{ij,nu-1}^w - C_{ij,nu}^w)\right] \tag{12}$$

$$\left[\frac{\partial C_{ij1}^w}{\partial t}\right]_{\text{disp}} = \frac{2D/\Delta u_{ij}}{\nu(r_{ij2}^2 - r_{ij1}^2)}\left[2r_{ij1}(C_{ij}^g/K_H - C_{ij1}^w) + r_{ij2}(C_{ij2}^w - C_{ij1}^w)\right] \tag{13}$$

Define

$$C_{ij}^w = \frac{\sum_{k=1}^{n_u} \Delta v_{ijk} C_{ijk}^w}{\sum_{k=1}^{n_u} \Delta v_{ijk}} \tag{14}$$

as the average aqueous VOC concentration in the ijth volume element ΔV_{ij}. Then, on the scale of these large volume elements, advective transport is described by

$$\nu\left[\frac{\partial C^w}{\partial t}\right]_{\text{adv}} = -\nabla\cdot(\mathbf{v}^w C^w) \tag{15}$$

where $\mathbf{v}^w$ = superficial water velocity, so

$$\left[\frac{\partial C^w}{\partial t}\right]_{\text{adv}} = -\frac{1}{\nu}\nabla\cdot(\mathbf{v}^w C^w) \tag{16}$$

Let us assume that

$$\left[\frac{\partial C^w_{ijk}}{\partial t}\right]_{\text{adv}} = -\frac{1}{\nu}\nabla\cdot(\mathbf{v}^w C^w_{ij}) \tag{17}$$

i.e., that the large-scale advection affects all the small shells around an air tube equally. Let

$$\begin{aligned}
S(u) &= 0,\ u \le 0\\
&= 1,\ u > 0\\
A^{\mathrm{I}}_{ij} &= \text{area of inner surface of } \Delta V_{ij} = 2\pi R_i \Delta z\\
A^{\mathrm{O}}_{ij} &= \text{area of outer surface of } \Delta V_{ij} = 2\pi R_{i+1}\Delta z\\
A^{\mathrm{T}}_{ij} &= A^{\mathrm{B}}_{ij} = \text{areas of top and bottom surfaces of } \Delta V_{ij}\\
&= \pi(R^2_{i+1} - R^2_i)\\
v^{\mathrm{I}}_{ij} &= v^w_r[(i-1)\Delta R, (j-\tfrac{1}{2})\Delta z]\\
v^{\mathrm{O}}_{ij} &= v^w_r[i\Delta R, (j-\tfrac{1}{2})\Delta z]\\
v^{\mathrm{B}}_{ij} &= v^w_z[(i-\tfrac{1}{2})\Delta R, (j-1)\Delta z]\\
v^{\mathrm{T}}_{ij} &= v^w_z[(i-\tfrac{1}{2})\Delta R, j\Delta z]
\end{aligned}$$

where v^w_r and v^w_z are the r and z components of the superficial water velocity. As discussed in more detail in previous papers (Ref. 6, for example), the finite difference approximation to Eq. (16) is then given by

$$\begin{aligned}
\left|\frac{\partial C^w_{ijk}}{\partial t}\right|_{\text{adv}} = \frac{1}{\nu\Delta V_{ij}}\{&A^{\mathrm{B}}_{ij}v^{\mathrm{B}}_{ij}[S(v^{\mathrm{B}})C^w_{i,j-1} + S(-v^{\mathrm{B}})C^w_{ij}]\\
&+ A^{\mathrm{T}}_{ij}v^{\mathrm{T}}_{ij}[-S(-v^{\mathrm{T}})C^w_{i,j+1} - S(v^{\mathrm{T}})C^w_{ij}]\\
&+ A^{\mathrm{I}}_{ij}v^{\mathrm{I}}_{ij}[S(v^{\mathrm{I}})C^w_{i-1,j} + S(-v^{\mathrm{I}})C^w_{ij}]\\
&+ A^{\mathrm{O}}_{ij}v^{\mathrm{O}}_{ij}[-S(-v^{\mathrm{O}})C^w_{i+1,j} - S(v^{\mathrm{O}})C^w_{ij}]
\end{aligned} \tag{18}$$

Here $S(v^{\mathrm{B}})$ is to be read as $S(v^{\mathrm{B}}_{ij})$, etc.

The final expression which controls the C^w_{ijk} is then

$$\frac{dC^w_{ijk}}{dt} = \left[\frac{\partial C^w_{ijk}}{\partial t}\right]_{\text{disp}} + \left[\frac{\partial C^w_{ijk}}{\partial t}\right]_{\text{adv}} \tag{19}$$

The movement of VOC in the advecting gas is described as follows. First, there is a source term corresponding to diffusion/dispersion of VOC into the gas from the water surrounding the air tubes. This is given by

$$n_{ij}\nu\pi a^2\Delta z\left[\frac{\partial C^g_{ij}}{\partial t}\right]_{\text{disp}} = -n_{ij}\frac{2\pi\Delta z Da}{\Delta u_{ij}}2(C^g_{ij}/K_{\text{H}} - C^w_{ij1})$$

or

$$\left[\frac{\partial C^g_{ij}}{\partial t}\right]_{\text{disp}} = -\frac{4D}{\nu a\Delta u_{ij}}(C^g_{ij}/K_{\text{H}} - C^w_{ij1}) \tag{20}$$

The terms associated with advective air transport are as follows. Let the volumetric air fluxes at the Inner, Outer, Bottom, and Top of ΔV_{ij} be U^{I}_{ij}, U^{O}_{ij}, U^{B}_{ij}, and U^{T}_{ij}, where these are calculated as described earlier (6). We assume that the total pressure at the point (R, z) is given by the ambient plus the hydrostatic pressure, so

$$P(R, z) = P(z) = P_0 + \sigma(h - z) \tag{21}$$

where h = aquifer thickness and $\sigma = 0.09675$ atm/m. Then

$$\begin{aligned} n_{ij}\nu\pi a^2\Delta z\left[\frac{\partial C^g_{ij}}{\partial t}\right]_{\text{adv}} &= A^{\text{I}}_{ij}U^{\text{I}}_{ij}[S(U^{\text{I}})C^g_{i-1,j} + S(-U^{\text{I}})C^g_{ij}] \\ &+ A^{\text{O}}_{ij}U^{\text{O}}_{ij}[-S(-U^{\text{O}})C^g_{i+1,j} - S(U^{\text{O}})C^g_{ij}] \\ &+ A^{\text{B}}_{ij}U^{\text{B}}_{ij}\left[S(U^{\text{B}})\frac{P[(j-1)\Delta z]}{P[(j-\frac{3}{2})\Delta z]}C^g_{i,j-1} + S(-U^{\text{B}})\frac{P[(j-1)\Delta z]}{P[(j-\frac{1}{2})\Delta z}C^g_{ij}\right] \\ &+ A^{\text{T}}_{ij}U^{\text{T}}_{ij}\left[-S(-U^{\text{T}})\frac{P[j\Delta z]}{P[(j+\frac{1}{2})\Delta z]}C^g_{i,j+1} - S(U^{\text{T}})\frac{P[j\Delta z]}{P[(j-\frac{1}{2})\Delta z]}C^g_{ij}\right] \end{aligned} \tag{22}$$

describes VOC advective transport in the gas phase. So

$$\left|\frac{\partial C^g_{ij}}{\partial t}\right|_{\text{adv}} = \frac{1}{n_{ij}\nu\pi a^2\Delta z}\left\{A^{\text{I}}_{ij}U^{\text{I}}_{ij}[S(U^{\text{I}})C^g_{i-1,j} + S(-U^{\text{I}})C^g_{ij}]\right.$$

$$+ A_{ij}^{O} U_{ij}^{O}[-S(-U^{O})C_{i+1,j}^{g} - S(U^{O})C_{ij}^{g}]$$

$$+ A_{ij}^{B} U_{ij}^{B}\left[S(U^{B})\frac{P[(j-1)\Delta z]}{P[(j-\frac{3}{2})\Delta z]}C_{i,j-1}^{g} + S(-U^{B})\frac{P[(j-1)\Delta z]}{P[(j-\frac{1}{2})\Delta z}C_{ij}^{g}\right]$$

$$+ A_{ij}^{T} U_{ij}^{T}\left[-S(-U^{T})\frac{P[j\Delta z]}{P[(j+\frac{1}{2})\Delta z]}C_{i,j+1}^{g} - S(U^{T})\frac{P[j\Delta z]}{P[(j-\frac{1}{2})\Delta z]}C_{ij}^{g}\right]\Bigg\} \tag{23}$$

describes the effect of advective transport on the gas phase VOC concentration in the ijth volume element. Finally,

$$\frac{dC_{ij}^{g}}{dt} = \left[\frac{\partial C_{ij}^{g}}{\partial t}\right]_{\text{disp}} + \left[\frac{\partial C_{ij}^{g}}{\partial t}\right]_{\text{adv}} \tag{24}$$

The model then consists of the following equations. First, dispersion in the aqueous phase is described by Eqs. (11), (12), and (13). Advection in the aqueous phase is described by Eqs. (14) and (18). The master equation for VOC concentrations in the aqueous phase is Eq. (19). Dispersion of VOC to the gas phase is described by Eq. (20); advective transport of VOC in the gas phase, by Eq. (23). The master equation for VOC concentrations in the gas phase is Eq. (24).

The equations for the molar air flux, the volumetric air flux, and the superficial water circulation velocity were discussed in detail previously (5, 6). We give them here, and refer the reader to the earlier papers for their development. Symbols are as follows.

Q = molar air flow rate of sparging well, mol/s
h = thickness of aquifer, m
a_0 = maximum radial distance from the sparging well at which gas is flowing at the top of the aquifer, m
R = gas constant, m^3·atm/mol·deg
T = temperature, °K
$P(z)$ = pressure at cylindrical coordinates (r, z), atm; see Eq. (22)

The r and z components of the molar air flux are given by

$$q_r = \frac{Qh^2 r}{\pi a_0^4 z^3}[a_0^2(z/h) - r^2] \tag{25}$$

$$q_z = \frac{2Qh^2}{\pi a_0^4 z^2}[a_0^2(z/h) - r^2] \tag{26}$$

The r and z components of the volumetric air flux are then given by

$$U_r = q_r RT/P(z)$$
$$U_z = q_z RT/P(z) \tag{27}$$

The r and z components of the superficial velocity associated with the water circulation induced by the injected air are taken to be

$$v_r^w = -(Bb/2)(h - 2z)r \cdot \exp(-2r/b) \tag{28}$$

$$v_z^w = Bz(h - z)(b - r) \cdot \exp(-2r/b) \tag{29}$$

where B = a scale factor measuring the coupling between the air flow and the water circulation rate, $1/(s \cdot m^2)$

b = distance from the well at which v_z^w changes from positive to negative, m

When the model was run it was found that the differential equations describing the change with time of the gas-phase VOC concentrations were extremely stiff, permitting the use of values of Δt no larger than 0.05–0.1 second. This led to extremely lengthy computer runs, since typically time periods of a month or more needed to be simulated. We therefore made the steady-state approximation for the equations describing the evolution of the gas-phase VOC concentrations, namely

$$\frac{dC_{ij}^g}{dt} = 0 = \left[\frac{\partial C_{ij}^g}{\partial t}\right]_{\text{adv}} + \left[\frac{\partial C_{ij}^g}{\partial t}\right]_{\text{disp}} \tag{30}$$

This equation is then solved for C_{ij}^g in terms of $C_{i,j-1}^g$, $C_{i-1,j}^g$, and C_{ij1}^w. Conveniently for ease of computation, the coefficients of $C_{i,j+1}^g$ and $C_{i+1,j}^g$ vanish for the gas flow field used. The result is that the stiff differential equations are replaced by a very tractable set of algebraic equations. We have utilized the steady-state approximation a number of times previously (Refs. 8 and 9, for example) and found it to be extremely useful. Use of the steady-state approximation permitted the use of Δt values of 25 to 100 seconds. Runs required from 20 minutes to 1 hour and 30 minutes on a personal computer equipped with an 80486 microprocessor and running at 50 MHz.

RESULTS

Runs were made to explore the dependence of the modeling results on the parameter K, which controls the number of air channels per unit area (see Eq. 1); the dispersion constant D; the Henry's constant of the VOC K_H; the parameter B controlling the rate of air-induced water circulation

(see Eqs. 28 and 29); and the linked air flow rate q and water circulation rate (assumed proportional to the air flow rate). Default values of the parameters for the runs shown in Figs. 4–8 are given in Table 1; other parameters are as indicated in the figure captions.

In Fig. 4 plots of normalized total residual mass VOC $M(t)/M_0$ are plotted versus time to show the effect of K, the proportionality constant governing the number of air channels per unit area in the domain of interest. The larger the value of K, the larger the number of air channels and the smaller the distances between them. In these runs the water circulation parameter B was set equal to zero. The larger the value of K, the shorter the distances across which dispersion must move VOC in order for it to reach an air channel and be removed, and the more efficient the dispersion process will be. As expected, we find that cleanup rates are drastically increased as K increases.

Figure 5 illustrates the effect of the diffusion/dispersion constant D on the rate of VOC removal by sparging. For these runs the cleanup rate is essentially proportional to the value of D. One cannot control the rate of molecular diffusion, but one can probably increase the rate of dispersion quite substantially by pulsing the air flow rate in the sparging well. This appears to have the potential for greatly accelerated remediations at very little cost; such extra costs as one might expect should be more than compensated for by decreased cleanup times.

TABLE 1
Default Parameters Used in the Model Calculations

Radius of the domain of interest	10 m
Thickness of the aquifer	8 m
Radius of influence of the sparging gas at the surface of the aquifer	8 m
Temperature	15°C
Volumetric air flow rate q in sparging well	5 SCFM, 0.00236 m^3/s
Water circulation length parameter b	5 m
Water circulation air flow coupling parameter B	0 $m^{-2} \cdot s^{-1}$
Air channeling parameter K	5×10^{-4} $s/m^2 \cdot mol$
Mean diameter of air channels in the aquifer	1 cm
Porosity of aquifer medium, dimensionless	0.3
Henry's constant of VOC (TCE), dimensionless	0.2821
Dispersivity of VOC in aquifer during sparging	2×10^{-7} m^2/s
Initial concentration of VOC in groundwater	100 mg/L
Radius and depth of contaminated zone	5 m, 4 m
n_r, n_z, n_u	10, 8, 6
Δt	25, 50, 100 seconds
Initial total mass of VOC	9.421 kg

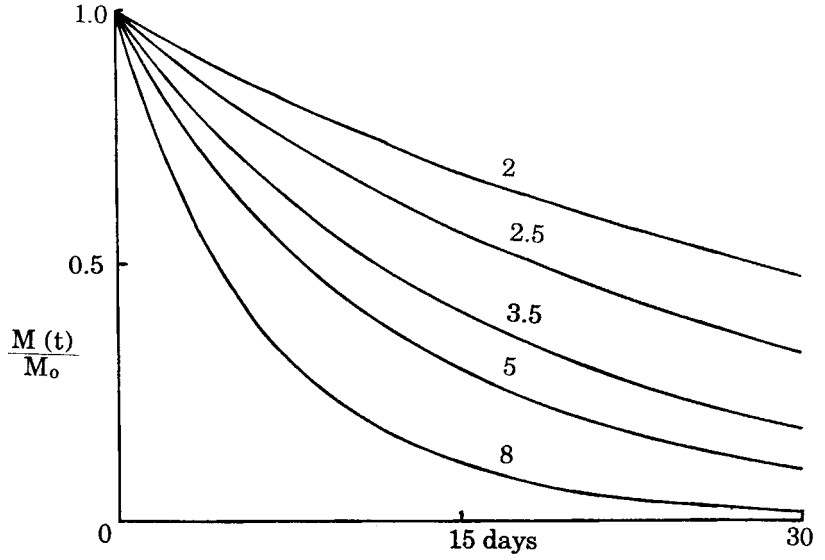

FIG. 4 Plots of normalized mass of residual VOC versus time; effect of K, which controls the number of air channels per unit area. From top to bottom, K = 2, 2.5, 3.5, 5, and 8 × 10^{-4} s/m^2·mol; other parameters as in Table 1.

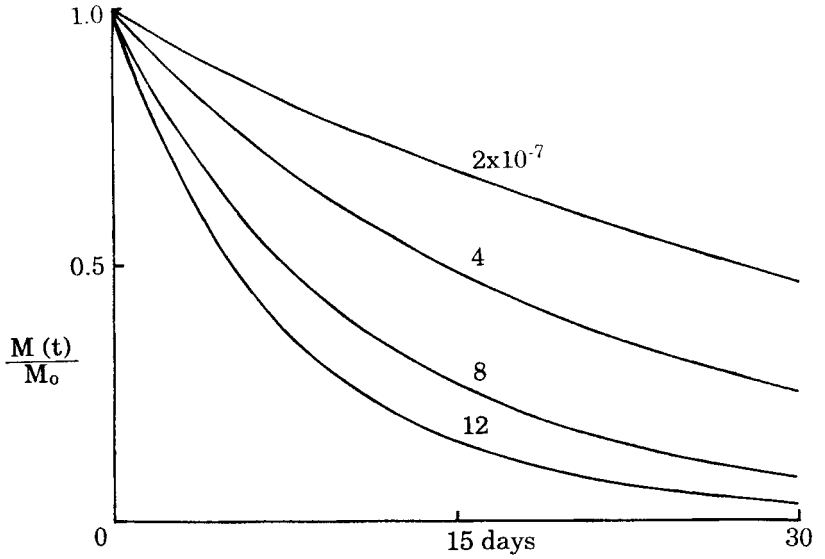

FIG. 5 Plots of normalized mass of residual VOC versus time; effect of D, the dispersion constant of the VOC during sparging. From top to bottom, D = 2, 4, 8, and 12 × 10^{-7} m^2/s; other parameters as in Table 1.

Under the operating conditions modeled here, the effect of the Henry's constant of the VOC is rather slight, as seen in Fig. 6. This is in agreement with the findings of the Sellers–Schreiber model (4), which predicts that cleanup rates should be independent of Henry's constant. Their model assumes that the sparging system is in the diffusion-limited regime of operation. We explore this point further later in this paper.

The proportionality constant B, which links the air flow rate to the magnitude of the water circulation rate, is a parameter which would be quite difficult to measure experimentally or to calculate theoretically. The results plotted in Fig. 7 are therefore very opportune, since they indicate that the dependence of cleanup rate on the value of B is quite weak. We see that the removal rate which results when $B = 0$ is not much less than that obtained when $B = 1 \times 10^{-4}\,m^{-2}\cdot s^{-1}$, which is in turn indistinguishable from that for $B = 2 \times 10^{-4}$. This result is in agreement with the results of an earlier more detailed study of the effect of B on VOC removal rates by sparging for a long horizontal well configuration (5).

The effects of changes in volumetric air flow rate q and proportional changes in water circulation parameter B are seen in Fig. 8. Linked increases in air flow and water circulation yield increased VOC removal rates because of the increased number of air channels and smaller domain

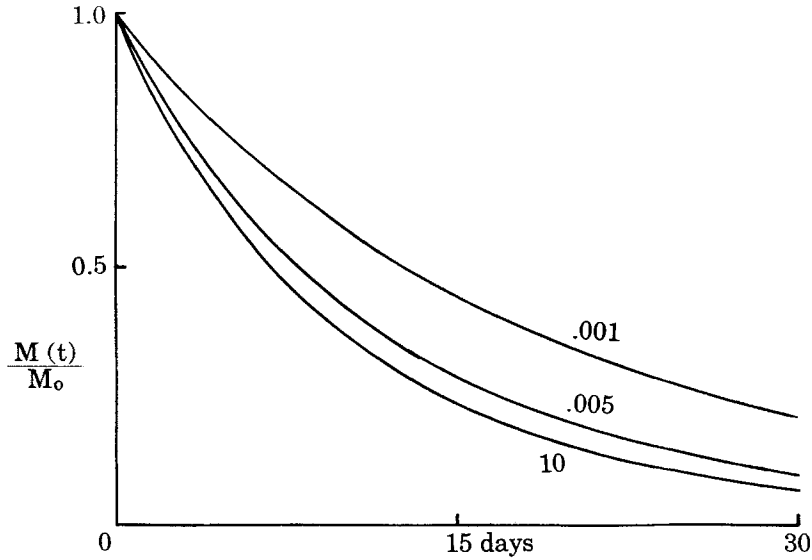

FIG. 6 Plots of normalized mass of residual VOC versus time; effect of Henry's constant of the VOC, K_H. From top to bottom, K_H = 0.001, 0.005, and 10; other parameters as in Table 1.

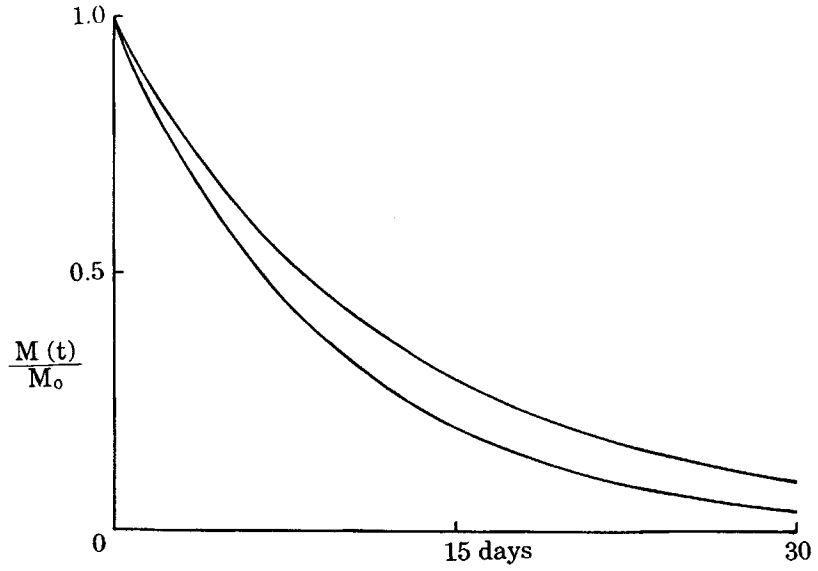

FIG. 7 Plots of normalized mass of residual VOC versus time; effect of the parameter B linking air flow rate to the water circulation rate. From top to bottom, $B = 0$, 1, and 2×10^{-4} $m^{-2} \cdot s^{-1}$ (superimposed).

radii implied by Eqs. (1) and (3). The increase in VOC removal rate with air flow in this model does not, however, necessarily indicate that the system is not diffusion-limited.

A SIMPLE SCREENING MODEL

Use of this model or others like it involves considerable effort, perhaps more than justified if only preliminary screening of sparging for use at a particular site is desired. Sellers and Schreiber have presented a simple screening model for getting upper limits to cleanup rates by sparging (4). Here we extend their treatment to cases in which the sparging is not strictly diffusion-controlled, and we use an improved method for calculating bubble residence times in the aquifer. The treatment is also extended to include the presence of nonaqueous phase liquid.

Contaminant Present Only as Dissolved VOC

This model, like that of Sellers and Schreiber, is a simple lumped parameter, one-compartment model for the preliminary screening of air sparging for in-situ groundwater remediation. It assumes that the contaminant is

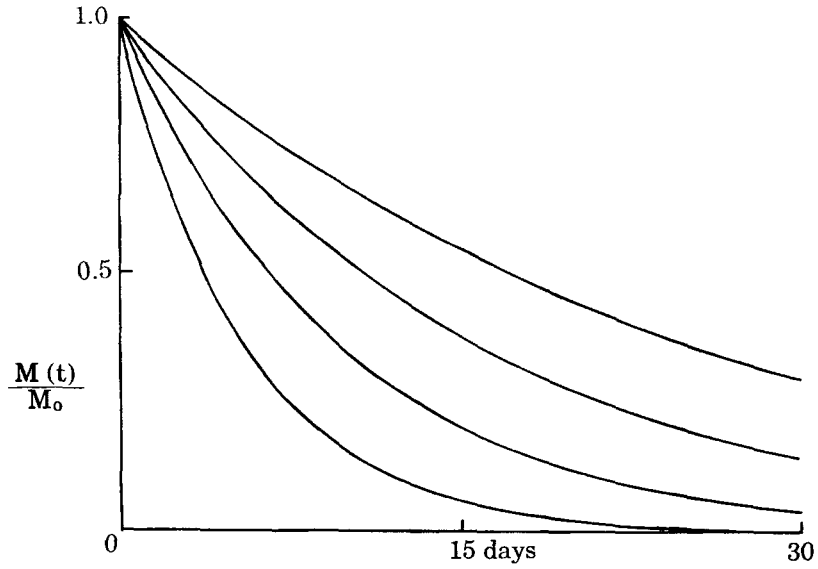

FIG. 8 Plots of normalized mass of residual VOC versus time; effect of linked volumetric air flow rate q and water circulation rate parameter B. From top to bottom, (q, B) = (2.5, 0.0001), (3.5, 0.00014), (5.0, 0.0002), and (7.5, 0.0003) (SCFM, $m^{-2} \cdot s^{-1}$). Other parameters as in Table 1.

present only as dissolved VOC. The model assumes an even distribution of air bubbles throughout the domain of influence of the well or, equivalently, complete mixing of the groundwater within the domain of influence. That is, the aquifer has a high permeability and a low chemical sorption capacity, and it is sufficiently homogeneous that good mixing of the groundwater in the domain of influence can be assumed. The model also assumes that there is no mixing of waters within and outside of the domain of influence, which is defined by the extent to which the bubbles spread laterally as they rise through the contaminated aquifer. This must be estimated experimentally. The sparging air is assumed to be incompressible. Lastly, the model assumes that there is no removal of VOC by biodegradation.

Terms are defined as follows:

t_t = bubble transit time across the aquifer, seconds, to be estimated later
a = bubble radius, m
$b - a$ = boundary layer thickness around bubble, m
q = volumetric air flow rate, m^3/s
V = volume of the domain of influence, m^3

ν = porosity of aquifer
K_H = Henry's constant of VOC, dimensionless
C_0 = initial average VOC concentration in the domain of influence, kg/m^3 of water

The number of bubbles generated per second, n, is given by

$$q = n(4\pi a^3/3)$$

so

$$n = 3q/(4\pi a^3) \tag{31}$$

We focus on a single bubble as it transits the domain of influence.

$m(t)$ = mass of VOC in bubble at time t; bubble is formed and released from the sparger at $t = 0$

Let us assume that there is equilibrium between the air in the bubble (assumed well-mixed) and the immediately adjacent portion of the surrounding water boundary layer with respect to VOC transport; see Fig. 9. Then

$$C(a) = \frac{3m}{4\pi a^3 K_H} \tag{32}$$

At steady state the VOC concentration in the boundary layer is given by

$$C(r) = A/r + B \tag{33}$$

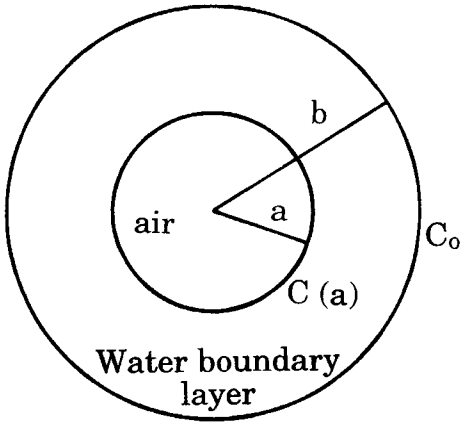

FIG. 9 Geometry and notation for mass transport of VOC through a boundary layer to a bubble.

where $C(r)$ = VOC concentration a distance r from the bubble center, $a < r < b$. Then

$$C(a) = A/a + B$$

and

$$C_0 = C(b) = A/b + B$$

from which we obtain

$$A = -[C_0 - C(a)]\frac{ab}{b - a} \tag{34}$$

and

$$\frac{dC}{dr} = \frac{ab[C_0 - C(a)]}{b - a}\frac{1}{r^2} \tag{35}$$

Fick's first law of diffusion then gives

$$\frac{dm}{dt} = 4\pi a^2 D\frac{ab[C_0 - C(a)]}{b - a}\frac{1}{a^2}$$

or

$$\frac{dm}{dt} = \frac{4\pi abD}{b - a}[C_0 - C(a)] \tag{36}$$

From Eq. (32) we have

$$m = (4\pi a^3/3)K_H C(a) \tag{37}$$

which on substitution into Eq. (36) and simplification yields

$$\frac{dC(a)}{dt} = \frac{3bD}{a^2(b - a)K_H}[C_0 - C(a)] \tag{38}$$

Let

$$\alpha = \frac{3bD}{a^2(b - a)K_H} \tag{39}$$

Then the solution to Eq. (38) which satisfies the requirement that $C(a) = 0$ at $t = 0$ is

$$C(a) = C_0[1 - \exp(-\alpha t)] \tag{40}$$

The concentration of VOC in the bubble as it leaves the aquifer at time t_t is readily obtained from Eq. (40); substitution of this result into Eq. (37)

gives

$$m(t_t) = \frac{4\pi a^3}{3} K_H C_0 \left\{1 - \exp\left[-\frac{3bDt_t}{a^2(b-a)K_H}\right]\right\} \tag{41}$$

Equation (41) gives the mass of VOC removed by one bubble; n bubbles are released per second, where n is given by Eq. (31). Let M = total mass of VOC in the domain of influence, kg. Then

$$M(t) = vVC(t) \tag{42}$$

where $C(t)$ = average VOC concentration in the domain of influence at time t, kg/m^3 of water, and

$$dM/dt = -nm(t_t) \tag{43}$$

Substitution of Eqs. (31), (41), and (42) into Eq. (43) and rearranging then yields

$$\frac{dC(t)}{dt} = -\frac{qK_H}{vV}\left\{1 - \exp\left[-\frac{3bDt_t}{a^2(b-a)K_H}\right]\right\} C(t) \tag{44}$$

Let

$$\beta' = \frac{qK_H}{vV}\left\{1 - \exp\left[-\frac{3bDt_t}{a^2(b-a)K_H}\right]\right\} \tag{45}$$

Then integration of Eq. (44) yields

$$C(t) = C_0 \cdot \exp(-\beta' t)] \tag{46}$$

In the limit as

$$\frac{3bDt_t}{a^2(b-a)K_H} \ll 1$$

(i.e., strict diffusion control), we obtain from Eq. (45)

$$\beta' = \frac{3qbDt_t}{vVa^2(b-a)} \tag{47}$$

which is Sellers and Schreiber's result; the removal rate of the VOC is independent of K_H under these conditions. If

$$\frac{3bDt_t}{a^2(b-a)K_H} \gg 1$$

that is, the process is equilibrium-controlled, we have

$$\beta' = qK_H/vV \tag{48}$$

and find that the removal rate is independent of D, b, and a, as expected.

A procedure somewhat different than that employed by Sellers and Schreiber is used to estimate the bubble rise velocities, needed to obtain the bubble transit times t_t. Bubble rise velocities were calculated as follows. Let

u = bubble rise velocity, cm/s
ρ = density of water, g/cm^3
μ = viscosity of water, poise
a = bubble radius, cm
g = gravitational constant, cm/s^2
N_{Re} = bubble Reynolds number, dimensionless
C = drag coefficient, dimensionless

The Reynolds number, bubble rise velocity (in free water), and drag coefficient are related as follows:

$$N_{Re} = 2au\rho/\mu \tag{49}$$

$$u = (8ag/3C)^{1/2} \tag{50}$$

$$\log_{10} C = -\frac{X}{1 + \exp[B(X - X_0)]} + C' \tag{51}$$

where $X = \log_{10} N_{Re}$
$B = 0.560$
$C' = 1.4976$
$X_0 = 3.6725$

Equation (50) is obtained from Perry and Chilton's Eq. (5-211) by assuming that the density of air is negligible compared to that of water, and that the bubbles are spherical; see Reference 7. Equation (51) was obtained by a numerical least-squares fit to the graph of $\log_{10} C$ versus $\log_{10} N_{Re}$ provided in Perry and Chilton (7); the plot was fitted over the range $-4 < \log_{10} N_{Re} < 4$.

Equations (49)–(51) were solved iteratively to generate a plot of bubble rise velocity in free water versus bubble diameter $d = 2a$ for $0 < d < 0.5$ cm; see Fig. 10. Stokes' law does not provide an adequate approximation for bubbles of realistic size, as seen in Fig. 11. A commonly used approximation for the drag coefficient in the transition flow region, $C =$

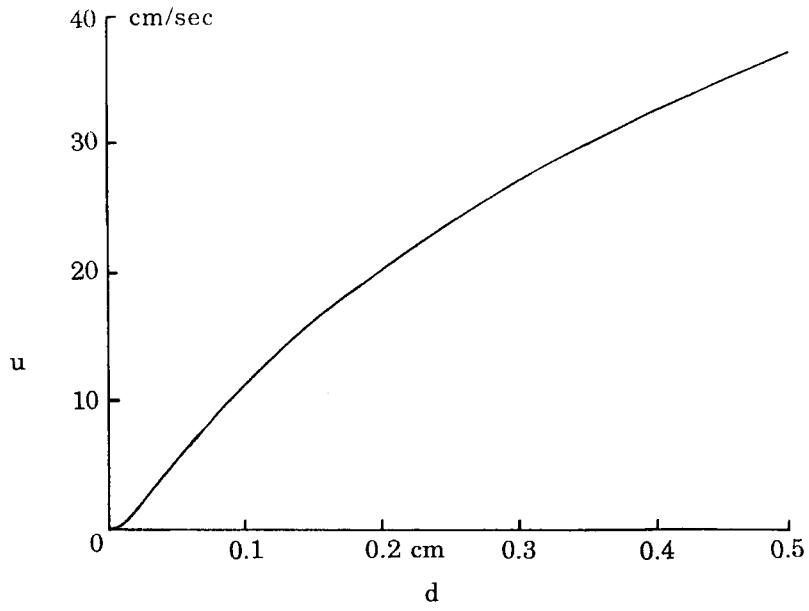

FIG. 10 Dependence of bubble rise velocity u (cm/s) on bubble diameter d (cm). Equations (49), (50), and (51) were solved simultaneously by interation for the Reynolds number, the bubble rise velocity, and the drag coefficient C.

$18.5/(N_{Re})^{0.6}$, fares somewhat better, as shown in Fig. 12, and would probably be regarded as adequate for $d < 0.2$ cm.

Another aspect of the bubble rise velocity which must be addressed is the effect of the finite sizes of the apertures in the aquifer through which the bubbles are moving. This point is discussed by Perry and Chilton (7). Figure 13 shows a plot of the wall correction factor, K_w, versus the ratio of bubble diameter d to aperture diameter d_a for bubbles in the Stokes' law regime. K_w is the factor by which the bubble rise velocity in free water must be multiplied to obtain the bubble rise velocity in an aperture. Figure 13 also shows a plot of the wall correction factor K'_w for bubbles in the Newton's law (turbulent flow) region. These plots indicate that use of velocities calculated for freely rising bubbles is very likely to seriously underestimate the transit time t_t of the bubbles moving across the aquifer. This, in turn, may lead to substantial underestimates of the efficiency of sparging. A reasonable but conservatively low estimate of the transit time would be obtained by using K'_w in Fig. 13 for the wall correction factor. Since low transit times result in low sparging efficiencies, this aspect of the modeling calculation would not be overoptimistic.

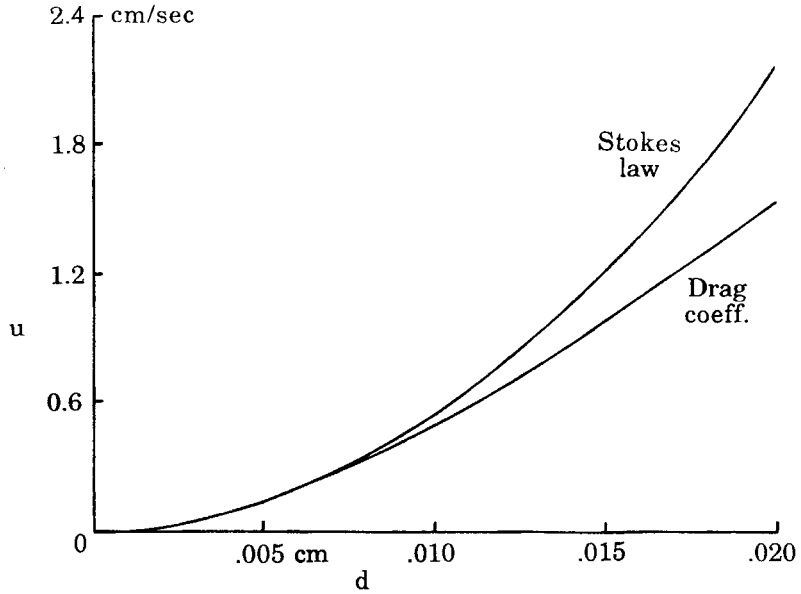

FIG. 11 Comparison of bubble rise velocities u calculated by Stokes' law and by Eqs. (49), (50), and (51). Note that the scales of this figure and of Fig. 12 differ from that of Fig. 11.

Contaminant Present as Dissolved VOC and NAPL

In this section we extend the sparging screening model to permit its application to situations in which nonaqueous phase liquid is present in the aquifer. Notation is as in the last section, with the following additions.

C_0^N = initial NAPL concentration, kg/m^3 of medium
C^N = NAPL concentration at time t, kg/m^3 of medium
ρ = density of NAPL, kg/m^3
α_0 = initial NAPL droplet radius, m
α = NAPL droplet radius at time t, m
$b - \alpha$ = diffusion boundary layer thickness around a NAPL droplet, m
b = one-half the distance between droplets, m
C_s = aqueous solubility of VOC, kg/m^3 of water
m_0 = initial mass of a NAPL droplet, kg
m = mass of a NAPL droplet at time t, kg
n = number of NAPL droplets per m^3 of medium, m^{-3}

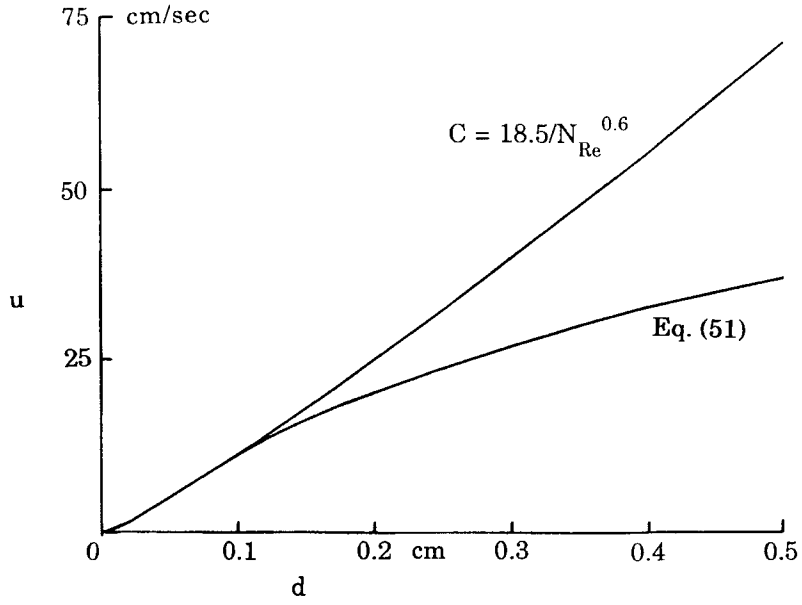

FIG. 12 Comparison of bubble rise velocities u calculated using a simple approximation for the drag coefficient ($C = 18.5/N_{Re}^{0.6}$) and using Eq. (51).

The solution of a spherical NAPL droplet in contact with an aqueous phase is handled as follows. The steady-state concentration of VOC in the vicinity of the droplet is readily shown to be given by

$$C(r) = A/r + B, \qquad \alpha < r < b \tag{52}$$

where r is the distance from the center of the droplet. The boundary conditions are

$$C(\alpha) = C_s \tag{53}$$

$$C(b) = C^w \tag{54}$$

where C^w is the bulk aqueous VOC concentration, kg/m^3. Use of the boundary conditions in Eq. (52) gives

$$A = \frac{(C_s - C^w)\alpha b}{b - \alpha} \tag{55}$$

Then dC/dr is given by

$$\frac{dC}{dr} = -\frac{(C_s - C^w)\alpha b}{b - \alpha}\frac{1}{r^2} \tag{56}$$

Use of Fick's law of diffusion then gives for the rate of mass loss of a

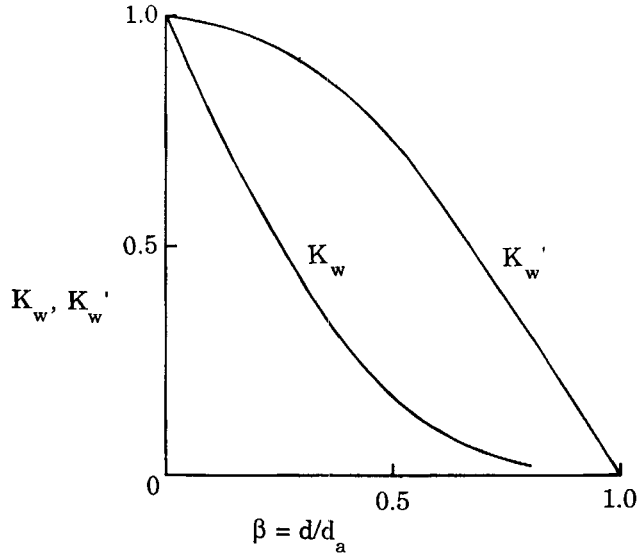

FIG. 13 Plots of wall correction factors K_w (for the Stokes' law regime) and K_w' (for the Newton's law regime) versus the ratio β of bubble diameter d to aperture diameter d_a. The rise velocity of a bubble in an aperture is obtained by multiplying the rise velocity of a freely rising bubble by the appropriate value of K_w or K_w'.

droplet,

$$\frac{dm}{dt} = -\frac{4\pi D(C_s - C^w)\alpha b}{b - \alpha} \tag{57}$$

after some cancellation.

The mass of a droplet is given in terms of its radius by

$$m = (4\pi/3)\rho\alpha^3 \tag{58}$$

and initially

$$m_0 = (4\pi/3)\rho\alpha_0^3 \tag{59}$$

from which we obtain

$$\alpha = \alpha_0(m/m_0)^{1/3} \tag{60}$$

Substitution of this result in Eq. (57) then gives

$$\frac{dm}{dt} = -\frac{4\pi D(C_s - C^w)\alpha_0 b(m/m_0)^{1/3}}{b - \alpha_0(m/m_0)^{1/3}} \tag{61}$$

for the rate of change of droplet mass with time due to solution.

The number of droplets per m^3 of medium, n, is given by

$$C_0^N = nm_0, \qquad \text{or} \qquad n = C_0^N/m_0 \tag{62}$$

where m_0 is given by Eq. (59). We note that $m/m_0 = C^N/C_0^N$ and that $dC^N/dt = n \cdot dm/dt$; substitution of these in Eq. (61) then gives

$$\frac{dC^N}{dt} = -(C_0^N/m_0)\frac{4\pi D(C_s - C^w)\alpha_0 b(C^N/C_0^N)^{1/3}}{b - \alpha_0(C^N/C_0^N)^{1/3}} \tag{63}$$

The quantity b (related to the diffusion boundary layer thickness) is calculated as follows. First,

$$n(4\pi/3)b^3 = 1 \tag{64}$$

Use of Eqs. (60) and (62), followed by solution for b, then yields

$$b = \alpha_0(\rho/C_0^N)^{1/3} \tag{65}$$

An alternative approach, which assumes that the droplets are placed in a cubic grid array, yields a very similar result,

$$b' = \alpha_0(\pi\rho/6C_0^N)^{1/3} = 0.806b \tag{66}$$

We are now in position to complete the model. A mass balance on dissolved VOC developed along the lines described in the preceding section gives

$$\nu\frac{dC^w}{dt} = -\nu\beta' C^w - \frac{dC^N}{dt} \tag{67}$$

where

$$\beta' = \frac{qK_H}{\nu V}\left\{1 - \exp\left[-\frac{3b_b D t_t}{a_b^2(b_b - a_b)K_H}\right]\right\} \tag{45'}$$

and

a_b = bubble radius, m
$b_b - a_b$ = bubble boundary layer thickness, m

So the modeling equations are

$$\frac{dC^N}{dt} = -(C_0^N/m_0)\frac{4\pi D(C_s - C^w)\alpha_0 b(C^N/C_0^N)^{1/3}}{b - \alpha_0(C^N/C_0^N)^{1/3}} \tag{68}$$

and

$$\frac{dC^w}{dt} = -\beta' C^w - (1/\nu)\frac{dC^N}{dt} \tag{69}$$

One can make an assumption about the initial distribution of the VOC between the aqueous and NAPL phases, or one could make measurements of the initial values of C^N and C^w. The results of the modeling calculations appear to be quite insensitive to how one handles the initial distribution, so the following prescription has been used in the results presented below. Here C_0 is the initial average total concentration of VOC in the aquifer, kg/m^3 of medium. Then

$$C_0 = C_0^N + \nu C_0^w \tag{70}$$

If we assume that the distribution of VOC between the aqueous and non-aqueous phases is at equilibrium, we can proceed as follows.

$$\text{If } C_0 \leq \nu C_s, \text{ then } C_0^w = C_0/\nu \text{ and } C_0^N = 0 \tag{71}$$

$$\text{If } C^0 > \nu C_s, \text{ then } C_0^w = C_s \text{ and } C_0^N = C_0 - \nu C_s \tag{72}$$

This assumption of equilibrium is often not valid, so it is fortunate that the modeling results are not sensitive to the initial distribution of VOC between the phases.

Equations (68) and (69) are strongly coupled, and Eq. (68) is nonlinear, so the prospects of an analytical solution for the model are poor. However, the system is quite easily and rapidly integrated numerically. The model was implemented in TurboBASIC and run on 80386 NX (20 MHz) and 80486 DX (50 MHz) microcomputers without any attempt at optimization of the time increment Δt used in the numerical integration; a typical run took a fraction of a minute of computer time.

Results Obtained with the Simple Screening Model

The dependence of the behavior of the simple screening model (with NAPL present) on several of the model parameters was explored. As mentioned earlier, one does not expect the screening model (which is a one-compartment model) to give highly realistic, quantitative results. It should, however, be useful in getting an intuitive, semiquantitative picture of what is going on and how changes in the various parameters describing a sparging operation can be expected to affect the rate of cleanup. Default values of the parameters used in these calculations are given in Table 2; when other values are used, they are given in the legends to the figures.

In Fig. 14 we see the effect on VOC removal rate of the depth into the aquifer to which the sparging well is drilled. Well depths in the aquifer are 6, 8, 10, and 12 m. The transit time t_t of a bubble in the aquifer is directly proportional to this well depth, and, as seen from Eq. (45), the longer the transit time, the more VOC is removed per bubble. The relationship is not a direct proportion, however, as was obtained by Sellers and

TABLE 2
Default Parameters Used in the Simple Screening Model for In-Situ Air Sparging

Volume of domain of influence	4000 m^3
Porosity of the aquifer domain	0.4
Pore diameter in aquifer	0.2 cm
Density of aquifer medium	1.7 g/cm^3
Depth of well in aquifer	10 m
Air flow rate	5 SCFM, 0.002360 m^3/s
Air bubble diameter	0.15 cm
Temperature	15°C
VOC simulated	Trichloroethylene, TCE
Solubility of VOC in water	1100 mg/L
Density of VOC	1.46 g/cm^3
Henry's constant of VOC, dimensionless	0.2821
Diffusion/dispersion constant of VOC in aquifer	2.0×10^{-10} m^2/s
NAPL droplet diameter	0.1, 0.4 cm
Initial VOC concentration	2000 mg/kg
Δt	50 seconds
Duration of run	750, 400 days, as indicated

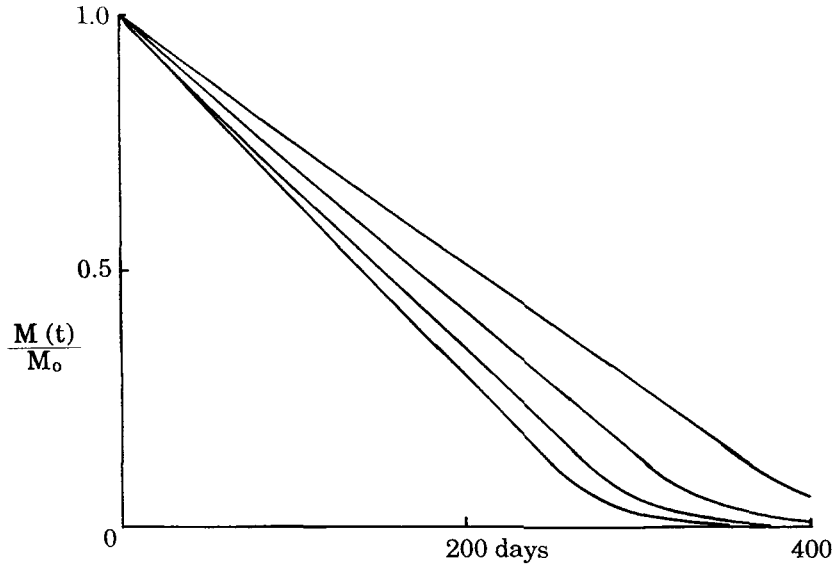

FIG. 14 Plots of residual reduced mass of VOC $M(t)/M(0)$ versus time; effect of aquifer thickness. NAPL droplet diameter = 0.1 cm; aquifer thickness = 6, 8, 10, and 12 m, top to bottom; other parameters as in Table 2. Bubble rise velocity in free water = 16.06 cm/s; wall correction factor K'_w = 0.381; bubble transit times t_t = 98.0, 130.7, 163.3, and 196.0 seconds.

Schreiber, since their model includes the simplifying assumption that the system is strictly diffusion-limited, unlike the present model.

The effect of aquifer pore diameter (a measure of the coarseness of the sand or gravel of which the aquifer is composed) is shown in Fig. 15. Pore diameters of 0.175, 0.20, 0.25, 0.30, 0.40, 0.60, and 1.00 cm were used, and the bubble diameter was 0.15 cm. As the pore diameter increases, the ratio of bubble diameter to pore diameter decreases, and the bubble rise velocity in the porous medium increases; see the plot of K'_w in Fig. 13. The transit time t_t is inversely proportional to the bubble rise velocity, and VOC removal rate increases with increasing t_t, so we find that increased aquifer pore size results in decreased removal rates. As seen in Fig. 15, the plots of $M(t)/M_0$ approach a limiting form as the pore diameter increases, since K'_w approaches a limiting value of unity.

One expects that increasing the NAPL droplet initial diameter α_0 at constant initial NAPL concentration C_0^N should decrease the rate of removal, since this results in a decrease in the NAPL–aqueous phase interfacial area, which in turn reduces the rate of solution of the NAPL. The results plotted in Fig. 16 show that this is indeed the case. Initial NAPL

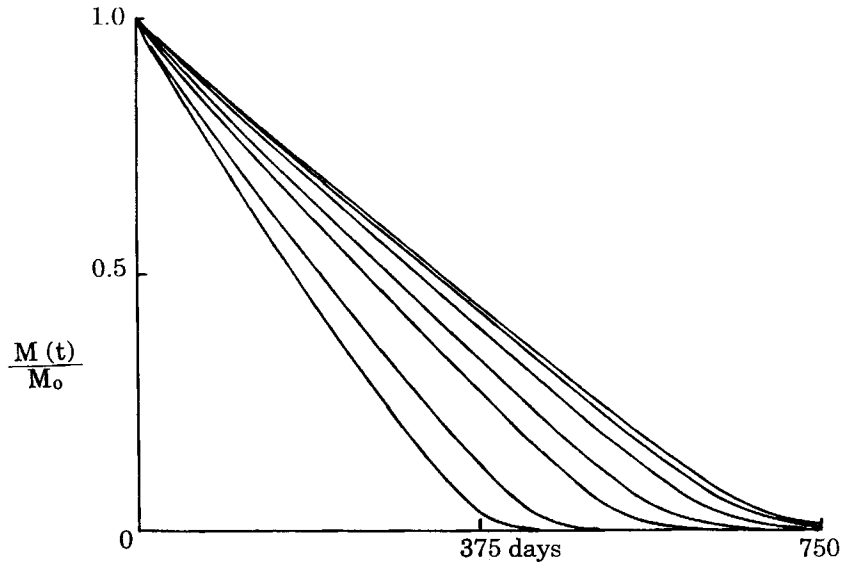

FIG. 15 Plots of residual reduced mass of VOC $M(t)/M(0)$ versus time; effect of aquifer pore diameter. NAPL droplet diameter = 0.4 cm; aquifer pore diameter = 1.0, 0.60, 0.40, 0.30, 0.25, 0.20, and 0.175 cm, top to bottom; other parameters as in Table 2. Bubble rise velocity in free water = 16.06 cm/s; (K'_w, t_t) = (0.977, 63.7), (0.936, 66.6), (0.851, 73.2), (0.728, 85.6), (0.602, 103.4), (0.381, 163.3), and (0.214, 291.3 seconds), top to bottom.

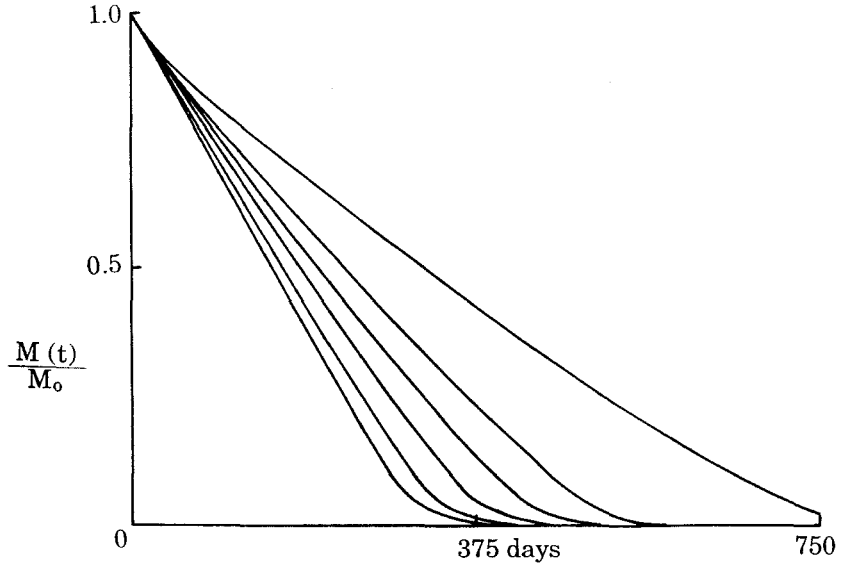

FIG. 16 Plots of residual reduced mass of VOC $M(t)/M(0)$ versus time; effect of NAPL droplet diameter. NAPL droplet diameter = 0.75, 0.50, 0.40, 0.30, 0.20, and 0.10 cm; other parameters as in Table 2. Bubble rise velocity in free water = 16.06 cm/s; K'_w = 0.381, t_r = 163.3 seconds.

droplet diameters here are 0.75, 0.5, 0.4, 0.3, 0.2, and 0.1 cm. For the smaller droplets the rate of solution appears to be sufficiently rapid that diffusion of dissolved VOC to the air bubbles is the principal rate-limiting factor, as indicated by the quite small difference between the plots for droplet diameters of 0.2 and 0.1 cm. We note that "droplet" should not be interpreted too literally here, especially when the "droplet diameters" are larger than the aquifer pore diameters. A more descriptive term might be "globs" or "ganglia" when the NAPL is squeezed into irregular shapes interstitially in the aquifer.

The runs plotted in Fig. 17 exhibit the effect of the initial average concentration of VOC, C_0, in the aquifer; values of C_0 are 2000, 1000, 500, and 250 mg/kg of aquifer medium. Note that the ordinate of these plots is $M(t)/M(0)$, so all plots start at (0, 1) even though the initial total masses $M(0)$ of VOC present are different. As expected, decreases in C_0 result in decreases in cleanup time. Cleanup time is not proportional to C_0, however, since the number of droplets, and therefore the NAPL–aqueous phase interfacial area, decrease proportionally with decreasing C_0. This, in turn, decreases the rate at which NAPL is dissolved. The plots for the higher values of C_0 exhibit a long linear or nearly linear region during

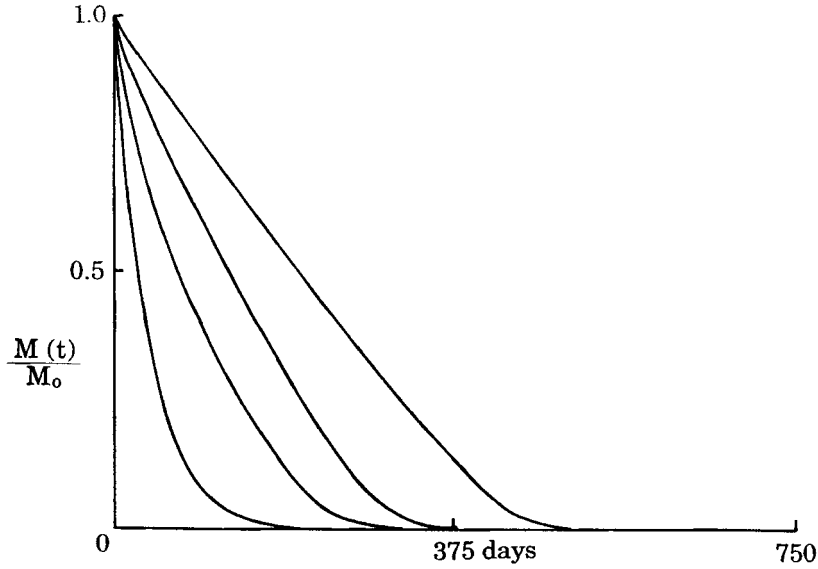

FIG. 17 Plots of residual reduced mass of VOC $M(t)/M(0)$ versus time; effect of initial VOC concentration. Initial NAPL droplet diameter = 0.4 cm; initial average total VOC concentration C_0 = 2000, 1000, 500, and 250 mg/kg of aquifer medium, right to left; other parameters as in Table 2. Bubble rise velocity in free water u = 16.06 cm/s; K'_w = 0.381; t_t = 163.3 seconds.

which NAPL is being dissolved, followed by an exponential tail after virtually all of the NAPL has been removed. At lower values of C_0, where less NAPL is present, the exponential tail becomes more and more important in determining the shape of the plots of $M(t)/M(0)$. No NAPL is present initially in the run for which C_0 = 250 mg/kg, and this plot shows the exponential decay which one would expect from Eq. (67) on setting $dC^N/dt = 0$.

Figures 18 and 19 show the effects of air bubble diameter on removal rate. In Fig. 18 the initial NAPL droplet diameter is 0.4, while in Fig. 19 it is 0.1 cm. Aquifer pore diameter is 0.20 cm for the runs in both figures, and the bubble diameters are 0.05, 0.10, 0.15, 0.175, and 0.19 cm. One expects that VOC removal rate should decrease with increasing bubble diameter, since the bubble rise velocity in free water increases with bubble diameter (see Fig. 10), so the transit time t_t should decrease. VOC removal rate decreases with decreasing t_t and decreasing air–water interfacial area, so it is not surprising that VOC removal rates decrease with increasing bubble diameter for bubble diameters of 0.05, 0.10, 0.15, and 0.175 cm. However, the VOC removal rate when the bubble diameter is 0.19 cm

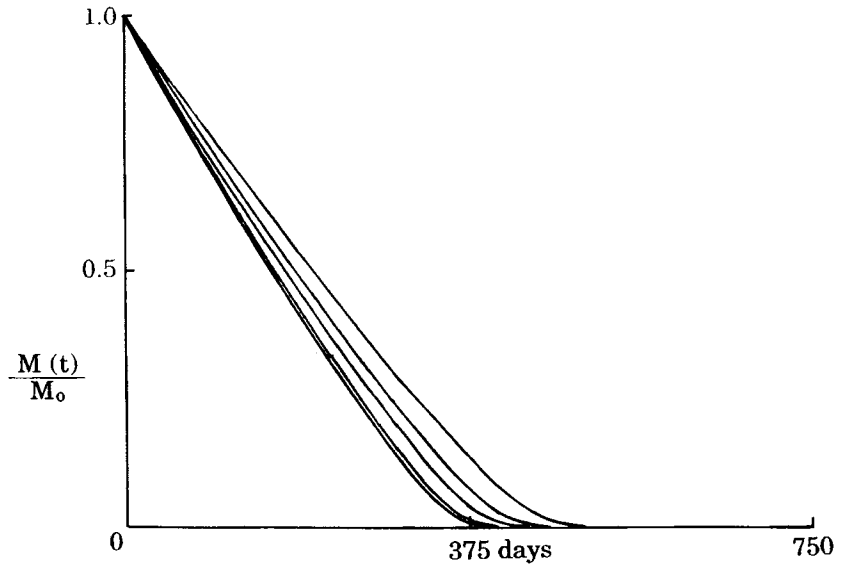

FIG. 18 Plots of residual reduced mass of VOC $M(t)/M(0)$ versus time; effect of air bubble size. Initial NAPL droplet diameter = 0.4 cm; air bubble diameter = 0.05, 0.19, 0.10, 0.15, and 0.175 cm, left to right. Other parameters as in Table 2. (u, K'_w, t_t) = (5.59, 0.936, 191.2), (19.51, 0.0724, 708.1), (11.17, 0.728, 123.0), (16.06, 0.381, 163.3), (18.26 cm/s, 0.186, 294.3 seconds), left to right.

reverses this trend, and is almost as fast as the removal rate when the bubble diameter is 0.05 cm. The reason for this apparent paradox is readily seen on examination of Fig. 13. For this run the bubble diameter (0.19 cm) is almost as large as the aquifer pore diameter (0.20 cm), and the wall correction factor K'_w for the bubble rise velocity is equal to only 0.0724. The bubble transit time for this run is 708 seconds, while the bubble transit times for the other runs range from 123 to 294 seconds.

Decreasing the NAPL droplet size from 0.4 to 0.1 cm and then varying the air bubble size produces the results shown in Fig. 19. Note the difference in time scale in the two figures; 400 days in Fig. 19, 750 days in Fig. 18. The same general tendency of VOC removal rate to decrease with increasing air bubble diameter that was seen in Fig. 18 is observed here, and again we see that the curve for which the bubble diameter is 0.19 cm is out of order in the sequence. The effect of bubble diameter is somewhat larger in Fig. 19 than in Fig. 18. This is presumably due to the fact that the rate of solution of VOC from the NAPL droplets is more rapid in the runs shown in Fig. 19 (droplet diameter 0.1 cm) than in the runs shown in Fig. 18 (droplet diameter 0.4 cm), so that the rate of diffusion of dis-

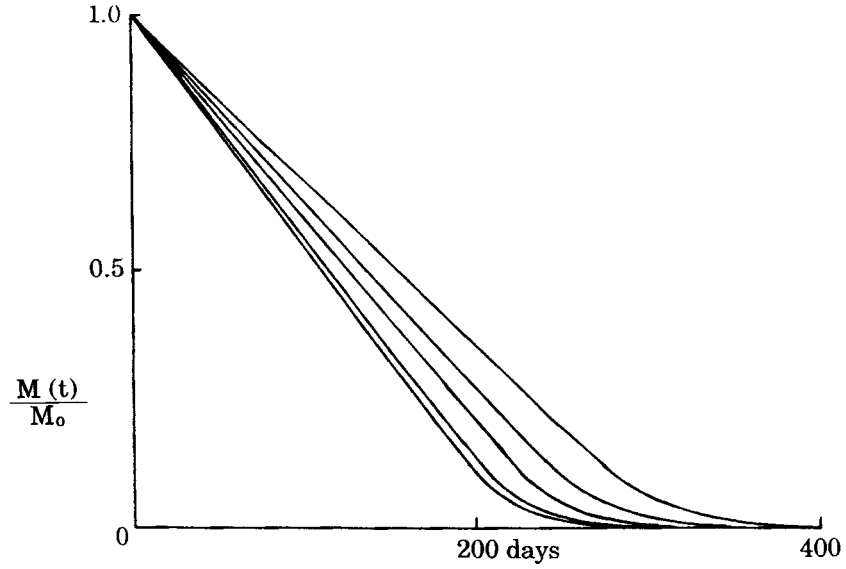

FIG. 19 Plots of residual reduced mass of VOC $M(t)/M(0)$ versus time; effect of air bubble size. Initial NAPL droplet diameter = 0.1 cm; air bubble diameter = 0.05, 0.19, 0.10, 0.15, and 0.175 cm, left to right. Other parameters as in Table 2. (u, K'_w, t_f) as in Fig. 18.

solved VOC to the air bubbles becomes more important as a rate-limiting factor.

CONCLUSIONS

A mathematical model for in-situ air sparging of dissolved organics from aquifers has been developed which includes the effects of air channeling along preferred paths in the aquifer. The dependence of the calculated results on the parameters of the model indicates that 1) wells should be designed to generate the maximum possible number of such air paths, and 2) wells should be operated in such a way as to generate the maximum amount of dispersive mixing. This second objective could probably be accomplished by pulsed air flow in the wells. A model parameter B, which links the air flow rate to the rate of water circulation and which would be difficult to measure or calculate, is shown to have rather little effect on calculated sparging cleanup rates, and can probably be assigned adequately by rough estimation.

The Sellers–Schreiber model for the preliminary screening of in-situ air sparging has been extended and modified to include the joint effects of Henry's law equilibrium and of diffusion transport, and to use an improved

method for calculating the bubble transit times across the aquifer. It also permits one to describe the removal of NAPL by sparging. The new version, a lumped parameter model like that of Sellers and Schreiber, is easily used and should be a useful tool for preliminary screening of the sparging technique. As is the case with other screening methods, it contains simplifying assumptions which limit its accuracy, and it should not be viewed as a substitute for the more detailed approaches needed for more precise evaluations and for design work.

ACKNOWLEDGMENTS

D.J.W. is greatly indebted to the University of Málaga for its hospitality and the use of its facilities, to Dr. J. J. Rodriguez-Jimenez for making his visit to Málaga possible, to Vanderbilt University for financial support during his leave, and to the Spanish Government (DGICYT) for a fellowship in support of this work.

REFERENCES

1. R. A. Brown, *Air Sparging: A Primer for Application and Design*, Groundwater Technology, Inc., 310 Horizon Center Dr., Trenton, New Jersey 08691. Undated.
2. A. N. Clarke, R. D. Norris, and D. J. Wilson, "Saturated Zone Remediation of VOCs through Sparging," in *Hazardous Waste Site Soil Remediation* (D. J. Wilson and A. N. Clarke, Eds.), Dekker, New York, 1993.
3. *Symposium on Soil Venting*, Houston, Texas, April 29–May 1, 1991, U.S. EPA Report EPA/600/R-92/174, 1992.
4. K. L. Sellers and R. P. Schreiber, "Air Sparging Model for Predicting Groundwater Cleanup Rate," in *Proceedings, Conference on Petroleum Hydrocarbons and Organic Chemicals in Ground Water: Prevention, Detection and Restoration. Eastern Regional Ground Water Issues*, Houston, Texas, November 4–6, 1992.
5. D. J. Wilson, J. M. Rodríguez-Maroto, and C. Gómez-Lahoz, "Groundwater Cleanup by In Situ Sparging. VI. A Solution/Distributed Diffusion Model for Nonaqueous Phase Liquid Removal," *Sep. Sci. Technol.*, *29*, 1401 (1994).
6. C. Gómez-Lahoz, J. M. Rodríguez-Maroto, and D. J. Wilson, "Groundwater Cleanup by In Situ Sparging. VII. VOC Concentration Rebound Caused by Diffusion after Shutdown", *Ibid.*, *29*, 1509 (1994).
7. R. H. Perry and C. H. Chilton (Eds.), *Chemical Engineer's Handbook*, 5th ed., McGraw-Hill, New York, 1973, pp. 5-61 to 5-65.
8. C. Gómez-Lahoz, J. M. Rodríguez-Maroto, and D. J. Wilson, "Biodegradation Phenomena During Soil Vapor Extraction: A High-Speed Non-Equilibrium Model," *Sep. Sci. Technol.*, *29*, 429 (1994).
9. J. M. Rodríguez-Maroto and D. J. Wilson, "Soil Cleanup by In Situ Aeration. VII. High-Speed Modeling of Diffusion Kinetics," *Ibid.*, *26*, 743 (1991).

Received by editor April 25, 1994